Energy-Driven Drag at Charge Neutrality in Graphene

Justin C. W. Song and Leonid S. Levitov

Phys. Rev. Lett. **109**, 236602 — Published 4 December 2012

DOI: 10.1103/PhysRevLett.109.236602

Energy-driven Drag at Charge Neutrality in Graphene

Justin C. W. Song[1,2] and Leonid S. Levitov[1]
[1] *Department of Physics, Massachusetts Institute of Technology, Cambridge, Massachusetts 02139, USA and*
[2] *School of Engineering and Applied Sciences, Harvard University, Cambridge, Massachusetts 02138, USA*

Coulomb coupling between proximal layers in graphene heterostructures results in efficient energy transfer between the layers. We predict that, in the presence of correlated density inhomogeneity in the layers, vertical energy transfer has a strong impact on lateral charge transport. In particular, for Coulomb drag it dominates over conventional momentum drag near zero doping. The dependence on doping and temperature, which is different for the two drag mechanisms, can be used to separate these mechanisms in experiment. We predict distinct features such as a peak at zero doping and a multiple sign reversal, which provide diagnostics for this new drag mechanism.

PACS numbers:

Vertical heterostructures comprised of a few graphene layers separated by an atomically thin insulating layer [1] afford new ways to probe the effects of electron interactions at the nanoscale. Typical layer separation d in these structures (1-2 nm) can be very small compared to the characteristic electron lengthscales such as the de Broglie wavelength, λ, and the screening length. This defines a new strong-coupling regime, $d \ll \lambda$, wherein the interlayer and intralayer interactions are almost equally strong. Fast momentum transfer between electron subsystems in the two layers and strong Coulomb drag have been predicted in this regime[2–7] with characteristic dependence on doping, temperature and layer separation distinct from that in previously studied systems[8].

Recent measurements[9, 10], while confirming theoretical predictions away from charge neutrality (CN), yield unexpected results at CN. Conventional momentum drag (P-mechanism) vanishes at CN because the sign of P-mechanism depends on the polarity of charge carriers[11]. However, experiment [10] shows a *sharp peak* in the drag response at CN. This disparity indicates that new physics is involved in driving drag in graphene at CN.

In this Letter, we propose a new mechanism for drag: energy-driven drag (E-mechanism). As we will show, E-mechanism becomes important in the *adiabatic regime* where the electronic system is thermally decoupled from the lattice. In graphene, slow electron-lattice cooling means that thermal decoupling persists over few-micron length scales even at room temperature[12–14]. As a result, electronic heat current is a dynamical variable, that together with charge current, governs transport behavior.

When $d \ll \lambda$, the interlayer electron-electron scattering mediates efficient vertical energy transfer between layers, which couples electron temperatures in the layers. In the adiabatic regime, coupled lateral energy flow in the two electronic systems, via thermoelectric effect, yields nonzero drag (see below). E-mechanism predicts drag which has a characteristic density dependence (illustrated in Fig. 1(b)) featuring a positive drag resistivity at double neutrality, $\rho_{21} > 0$. The sign, as well as the peak structure in ρ_{21}, agrees with experiment[10].

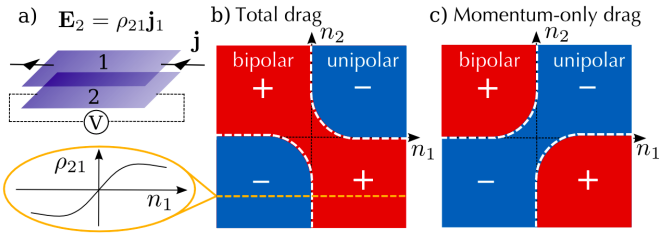

FIG. 1: Different mechanisms for Coulomb drag in graphene heterostructures. E-mechanism dominates over P-mechanism near zero doping, whereas P-mechanism dominates at higher doping. The sign of the drag response depends on carrier polarity (a). For potential fluctuations of equal sign in the two layers, Eq.(1), the net drag (b) features a pair of nodal lines (white dashed lines). Positive drag in the avoided crossing region at zero doping is dominated by E-mechanism. The resulting dependence is distinct from P-mechanism-only drag (c) smeared by correlated density fluctuations, $\delta\mu_1 \approx \delta\mu_2$.

E-mechanism arises due to the coupling between vertical energy transfer and lateral charge and energy transport via spatial density inhomogeneity which is intrinsic to graphene. Density inhomogeneity is known to be particularly strong at CN in the electron-hole puddle regime[15], providing the dominant disorder potential in clean samples. When a charge current is applied in layer 1, density inhomogeneity produces spatially varying heating/cooling [see Eq.(2)]. Strong thermal coupling between the electron systems in the two layers, mediated by the interlayer energy transfer, leads to a temperature pattern in layer 2 that tracks that in layer 1, $\delta T_2(r) \approx \delta T_1(r)$. Further, since the disorder correlation length $\xi_{\rm dis}$ can reach 100 nm in G/BN heterostructures[16, 17], exceeding the layer separation by orders of magnitude, the potential fluctuations are nearly identical in the two layers,

$$\langle \delta\mu_1(r)\delta\mu_2(r')\rangle > 0 \qquad (1)$$

for $r \approx r'$. As a result, the position-dependent thermopower induced by the gradient $\nabla\delta T_2(r)$ is correlated with the heating/cooling pattern in layer 1, giving rise to a nonzero ensemble-averaged drag voltage in layer 2.

Our mechanism predicts a particular sign of the energy

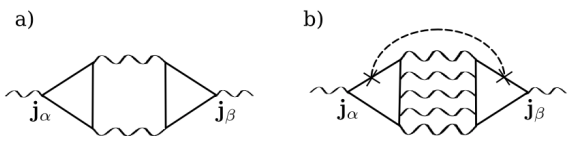

FIG. 2: Feynman diagrams for P-mechanism (a) and E-mechanism (b) for drag. Wavy lines represent interactions, dashed line represents disorder averaging. The ladder in (b) represents a long-wavelength charge-neutral mode.

contribution to drag. As a result, the density dependence for the net drag (E- and P-mechanism combined) features a split-up pattern of nodal lines with an "avoided crossing" at zero doping, as illustrated in Fig. 1 (b). The double sign change along the main diagonal $n_1 = n_2$ and the peak at $n_{1,2} = 0$ make E-mechanism easy to distinguish experimentally.

As a parenthetical remark, the correlated density inhomogeneity, Eq.(1), also affects the P-mechanism, however its effect is opposite to that of the E-mechanism. If P-mechanism were the dominant contribution near zero doping, the pattern of nodal lines would be such that the drag sign was constant along the main diagonal (see Fig.1b and c).

E-mechanism is mediated by neutral modes (particle-hole excitations, or electron-lattice temperature imbalance) which are of a long-range character, and thus can be described by a hydrodynamic approach. The relevant length scales for these modes are ξ_T and $\xi_{\rm dis}$, the electron-lattice cooling length and the inhomogeneity correlation length, respectively. For a long-range disorder potential and not too low temperatures, the lengthscales ξ_T and $\xi_{\rm dis}$ are larger than the inelastic mean free path, $\ell = v/\gamma$, where γ is the electron-electron scattering rate. As a result, E-mechanism is captured by a hydrodynamic framework which involves charge current $\mathbf{j}$ and heat current $\mathbf{j}_{\rm q}$, which in the ballistic transport regime are related by

$$\mathbf{j}_{\rm q}(\mathbf{r}) = Q(n)\mathbf{j}, \quad Q[n(\mathbf{r})] = \mathcal{S}[n(\mathbf{r})]T/e, \tag{2}$$

where $\mathcal{S}(n)$ is the entropy per carrier, $n(\mathbf{r})$ is the density profile, and $e < 0$ is the carrier charge. In the ballistic regime, using the electron temperature approximation, we find[18]

$$Q = \frac{2\pi^2 k_B^2 T^2 \mu}{3e(\mu^2 + \Delta^2(T))}. \tag{3}$$

where $\Delta(T)$ accounts for the Dirac point broadening due to disorder and thermal fluctuations.

It is instructive to compare the Feynman diagrams describing different mechanisms (see Fig.2). The characteristic momenta are fairly large for P-mechanism ($\sim k_F$), making it a local contribution. In contrast, E-mechanism includes ladder diagrams representing long-range modes propagating over distances of order $\xi_T \gg k_F^{-1}$.

To illustrate the relation between energy and charge transport, we first analyze in-plane resistivity in a single layer. According to Eq.(2), spatial inhomogeneity leads to heating/cooling in the presence of uniform charge current (as in the Joule-Thomson process). The spatial temperature profile can be found from $-\nabla\kappa\nabla\delta T + \lambda\delta T = -\nabla\cdot\mathbf{j}_{\rm q}$, where κ is the thermal conductivity and $\lambda\delta T$ is the electron-lattice cooling power. A temperature gradient $\nabla\delta T$ drives thermopower, providing additional dissipation and thereby increasing resistivity. Onsager reciprocity combined with Eq.(2) gives $\mathbf{E}(r) = -(Q[n(\mathbf{r})]/T)\nabla\delta T$[18]. Taking an ensemble average over small density fluctuations, $\delta\mu \ll k_B T, \mu$, we find an increase in the in-plane resistivity, $\langle\rho_{\alpha\beta}\rangle = \rho^0_{\alpha\beta} + \Delta\rho_{\alpha\beta}$, $[\alpha(\beta) = x, y]$, where

$$\Delta\rho_{\alpha\beta} = \frac{1}{T}\sum_{|\mathbf{q}|\lesssim 1/\ell} \frac{\langle\delta Q(-\mathbf{q})\delta Q(\mathbf{q})\rangle}{\kappa q^2 + \lambda} q_\alpha q_\beta. \tag{4}$$

Since the derivative $\partial Q/\partial\mu$ peaks at $\mu = 0$, this results in $\Delta\rho_{\alpha\beta}$ that peaks at CN. The temperature dependence estimated below is $\Delta\rho \propto T^2$, reminiscent of super-linear power laws for resistivity frequently observed at small doping[19]. A contribution of nonthermal modes to $\Delta\rho$ was analyzed in Ref.[20].

Generalizing this analysis to two layers coupled by vertical energy transfer and accounting for correlated density fluctuations, Eq.(1), we find an ensemble-averaged drag response $\mathbf{E}_2 = \rho_{21}\mathbf{j}_1$,

$$\rho_{21}^{(\rm e)} = \frac{1}{2T\tilde\kappa}\frac{\partial Q}{\partial\mu_1}\frac{\partial Q}{\partial\mu_2}\sum_{\mathbf{q}} \frac{\langle\delta\mu_2(-\mathbf{q})\delta\mu_1(\mathbf{q})\rangle}{1 + \tilde\ell^2\mathbf{q}^2}. \tag{5}$$

Here $\tilde\kappa = \kappa_1 + \kappa_2$ is the net thermal conductivity of the two layers, μ is the chemical potential, and $\tilde\ell$ is the interlayer cooling length. This length is estimated below and is shown to be of order of the inelastic mean free path, $\tilde\ell \sim \ell$, much shorter than the electron-lattice cooling length ξ_T. Because the sign of the correlator in Eq.(5) is positive, energy-driven drag has the same sign as $\Delta\rho_{\alpha\beta}$ in Eq.(4), i.e. is *positive at zero doping*. This results in a double sign change along the main diagonal $n_1 = n_2$, as pictured in Fig. 1 (b). The density dependence for $\rho_{21}^{(\rm e)}$ features a peak at zero doping (see Fig.3) which is a hallmark of the E-mechanism regime.

Positive correlation, Eq.(1), is expected for disorder potential dominated by charge impurities [21–23]. For the correlator $\langle\delta\mu_1\delta\mu_2\rangle$ of a negative sign, conjectured for strain-induced charge puddles[24], our analysis predicts a negative drag at zero doping. Hence drag is a useful tool for probing the origin of inhomogeneity in graphene.

We begin by studying the energy transfer between the electronic systems in the two layers (Fig.1(a)). This is described by the Hamiltonian

$$\mathcal{H} = \sum_i \int d^2\mathbf{r}\psi_i^\dagger(\mathbf{r})\Big[-i\hbar v\sigma\cdot\nabla + \delta\mu_i(\mathbf{r})\Big]\psi_i(\mathbf{r}) + \mathcal{H}_{\rm el-el} \tag{6}$$

where $i,j = 1...2N$ index layer, and spin/valley degrees of freedom, $\delta\mu(\mathbf{r})$ describes the slowly varying disorder potential, v is the Fermi velocity. The electron-electron interactions are described by $\mathcal{H}_{\rm el-el} = \frac{1}{2}\sum_{\mathbf{q},\mathbf{k},\mathbf{k}',i,j} V_{ij}(\mathbf{q})\psi^\dagger_{\mathbf{k}+\mathbf{q},i}\psi^\dagger_{\mathbf{k}'-\mathbf{q},j}\psi_{\mathbf{k}',j}\psi_{\mathbf{k},i}$.

In our analysis, we ignore the correction due to finite layer separation d, approximating the interlayer interaction by the bare Coulomb interaction, $V_{ij}(\mathbf{q}) \approx V^0_{\mathbf{q}} = 2\pi e^2/\varepsilon|\mathbf{q}|$ with ε the background dielectric constant. This approximation is valid when the lengthscale d is small compared to the screening length and Fermi wavelength in the layers, which is the case for systems of interest[1]. The random-phase approximation then yields a screened interaction $V_{ij}(\mathbf{q}) = V^0_{\mathbf{q}}/[1 - V^0_{\mathbf{q}}(\Pi_1(\mathbf{q},\omega) + \Pi_2(\mathbf{q},\omega))]$ for i,j in different layers.

We describe the energy distribution of carriers in each layer by a Fermi distribution at temperatures $T_{1,2}$. Using Fermi's golden rule we can calculate the rate of energy exchange between the two layers (see Appendix). In the degenerate limit $\mu_1, \mu_2 \gg k_BT$, we obtain the energy transfer rate between layers 1 and 2:

$$\mathcal{J}_{12} = \frac{6\zeta(4)}{\hbar^3 v^2}\frac{\nu_1\nu_2 k_B^4}{(\nu_1+\nu_2)^2}\left(T_1^4 \ln\frac{T_0}{T_1} - T_2^4\ln\frac{T_0}{T_2}\right) \qquad (7)$$

where $\nu(\mu)$ is the total density of states in each layer, and $k_BT_0 = v(2\pi e^2/\varepsilon)(\nu_1+\nu_2)$. Notably, for equal densities $\mathcal{J}_{12}$ does not depend on the Fermi surface size. For equal densities and small temperature differences between the layers $T_1 \approx T_2$, we obtain the cooling rate

$$\gamma = \frac{1}{C_{\rm el}}\frac{d\mathcal{J}_{12}}{dT} = \frac{9\zeta(4)k_B^2T^2}{\pi\mu\hbar}\ln\frac{T_0}{T} \qquad (8)$$

where the heat capacity $C_{\rm el} = \pi^2/3k_B^2T\nu(\mu)$ and the density of states $\nu(\mu) = 2\mu/(\pi\hbar^2v^2)$ for the degenerate limit have been used. The rate γ increases as μ goes towards neutrality, but is already quite large for μ away from neutrality. This is completely analogous to intralayer scattering [25, 26]. For typical values $\mu = 100\,$meV, $T = 300\,$K, the rate γ is about $30\,\mathrm{ps}^{-1}$, orders of magnitude faster than the electron-lattice cooling rates[12–14].

Vertical energy transfer couples heat transport in the two layers, so that the layer temperatures T_1, T_2 obey

$$\begin{aligned} -\nabla\kappa_1\nabla\delta T_1 + a(\delta T_1 - \delta T_2) + \lambda\delta T_1 &= -\nabla\cdot\mathbf{j}_{q,1} \\ -\nabla\kappa_2\nabla\delta T_2 + a(\delta T_2 - \delta T_1) + \lambda\delta T_2 &= 0 \end{aligned} \qquad (9)$$

where $a = d\mathcal{J}_{12}/dT$ [see Eq.(7)] and λ describes electron-lattice cooling. We consider only a response linear in the applied current, $\mathbf{j}$, neglecting the quadratic joule heating term. Inverting the coupled linear equations, we find an increase in temperature in layer 2, $\delta T_2(\mathbf{r})$, that is driven by current in layer 1 as

$$\delta T_2(\mathbf{r}) = -\frac{a}{\widehat{L}_1\widehat{L}_2 - a^2}(\mathbf{j}_1\cdot\nabla)Q[n_1(\mathbf{r}),T], \qquad (10)$$

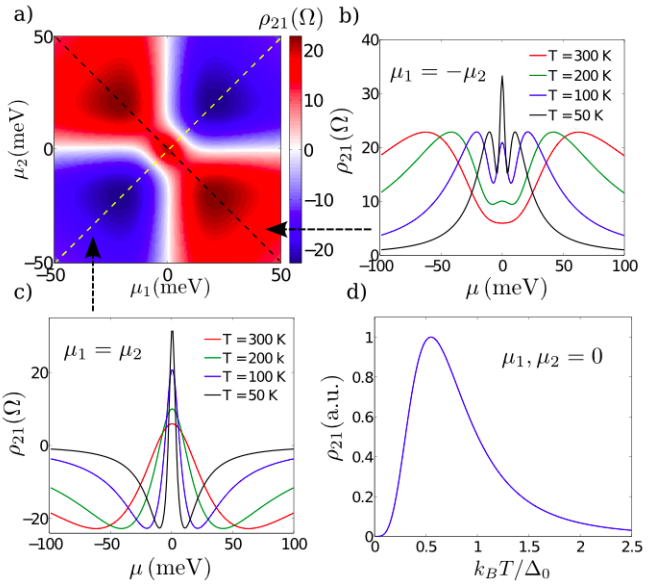

FIG. 3: (a) Total drag resistivity $\rho_{21}^{(\rm tot)} = \rho_{21}^{(\rm m)} + \rho_{21}^{(\rm e)}$ *vs.* chemical potentials in the two layers, evaluated from Eq.(11) and Eq.(5) at $T = 100\,$K, producing a peak at $\mu_{1,2} = 0$ (see text for parameter values used). (b,c) Slices $\mu_1 = \mu_2$ and $\mu_1 = -\mu_2$ at different temperatures. Note a three-peak structure in slice (b) and two sign changes close to CN in (c). (d) Temperature dependence of the peak at $\mu_{1,2} = 0$ in the diffusive regime.

where $\mathbf{j}_{q,1}$ is the heat current, Eq.(2), where $\widehat{L}_i = -\nabla\kappa_i\nabla + a + \lambda$. In what follows we suppress the λ term since electron-lattice cooling is slow. Eq.(10) then predicts a value for the interlayer cooling length $\tilde{\ell} = \sqrt{\kappa_1\kappa_2/[(\kappa_1+\kappa_2)a]}$, which yields a value close to that for the mean free path ℓ. The induced temperature profile, $\delta T_2(\mathbf{r})$, creates thermal gradients that can drive a local thermopower via $\mathbf{E}_2(r) = -(Q[n_2(\mathbf{r})]/T)\nabla\delta T_2$.

Spatial fluctuations in thermopower are governed by density fluctuations via Eq.(10). In particular, close to neutrality the local thermopower will exhibit regions of both positive and negative sign, leading to a spatial pattern of the drag resistivity. As discussed above, the correlations between $\delta\mu_1$ and $\delta\mu_2$, Eq.(1), lead to a nonzero ensemble-averaged drag resistivity. In the limit $\delta\mu_{1,2} \ll k_BT, \mu_{1,2}$ we write $Q_i(\mathbf{r}) = \langle Q_i(\mathbf{r})\rangle + \frac{\partial Q}{\partial\mu_i}\delta\mu_i(\mathbf{r})$. Passing to Fourier harmonics via $\langle\delta\mu_1(\mathbf{r})\delta\mu_2(\mathbf{r}')\rangle = \sum_{\mathbf{q}} e^{i\mathbf{q}(\mathbf{r}-\mathbf{r}')}\langle\delta\mu_1(-\mathbf{q})\delta\mu_2(\mathbf{q})\rangle$, we obtain Eq.(5).

The fact that fluctuating local thermopower, exhibiting both positive and negative signs, does not average to zero is surprising. This happens because the inhomogeneity in heat current and thermopower arise from the same source: electron-hole puddles. E-mechanism resembles mutual drag described by Laikhtman and Solomon [27] in semiconducting heterostructures where doping at contacts produced a similar correlation between Peltier heating/cooling and thermopower. E-mechanism in graphene differs from Ref.[27] in that density inhomogeneity is intrinsic, occurs throughout the sample (not just at the

contacts), and on a far smaller scale.

To see how E-mechanism, Eq.(5), affects the total experimentally measured drag we need to account for P-mechanism contribution. We use a model that captures the main qualitative features of momentum drag:

$$\rho_{21}^{(\mathrm{m})} = \tilde{\rho}_{21}^{(\mathrm{m})} \frac{h}{e^2} \frac{(k_B T)^2 \mu_1 \mu_2}{(\mu_1^2 + \eta k_B^2 T^2)(\mu_2^2 + \eta k_B^2 T^2)}, \qquad (11)$$

$\tilde{\rho}_{21}^{(\mathrm{m})} = -1.4\alpha^2/(2\pi\eta^2)$, where $\eta k_B^2 T^2$ describes thermal broadening of the Dirac point. This expression, with the effective interaction strength $\alpha = 0.05$, and $\eta = 6.25$, was obtained by fitting the functional dependence derived in Ref. [7] in the doping region $-10 < \mu/k_{\mathrm{B}}T < 10$.

Combining this with $\rho_{21}^{(\mathrm{e})}$ in Eq.(5), we obtain the total drag $\rho_{21}^{(\mathrm{tot})} = \rho_{21}^{(\mathrm{m})} + \rho_{21}^{(\mathrm{e})}$ plotted in Fig.3. Here we have used an estimate for thermal conductivity [28]

$$\kappa = b(\mu^2 + \Delta^2(T))/\hbar T, \quad \Delta^2(T) = \Delta_0^2 + \eta(k_B T)^2, \quad (12)$$

and assumed Gaussian correlations with average square density fluctuations $\langle \delta\mu^2 \rangle \approx 25\,\mathrm{meV}^2$ and $\xi_{\mathrm{dis}} = 100\,\mathrm{nm}$ [16, 17]. Here $\Delta(T)$ accounts for Dirac point broadening by disorder and thermal fluctuations [18], and b is a constant of order unity; its exact value does not impact the qualitative features seen in Fig. 3. We note that the details of the functional form of the correlator in Eq.(1) do not impact the qualitative behavior. The obtained values of total drag are compatible with measured drag resistivities reported in Refs.[9, 10].

The density dependence of total drag plotted in Fig.3 (a) can be used to distinguish the two drag mechanisms in experiments. Namely, the peak at zero doping is due to E-mechanism On the slice $\mu_1 = -\mu_2$ (black dashed line) this peak is surrounded by two peaks dominated by the momentum contribution [Fig.3(b)]. On the slice $\mu_1 = \mu_2$ (yellow dashed line) the two mechanisms produce contributions of opposite sign, resulting in a double sign change [Fig.3(c)]. This provides a clear means of discerning the E-mechanism regime.

The temperature dependence can be estimated as follows. At not too low T such that $\tilde{\ell}, \ell \lesssim \xi_{\mathrm{dis}}$, the sum in Eq.(5) yields $\sum_{\mathbf{q}} \langle \delta\mu_1(-\mathbf{q}) \delta\mu_2(\mathbf{q}) \rangle = \langle \delta\mu_1(\mathbf{r}) \delta\mu_2(\mathbf{r}') \rangle_{\mathbf{r}=\mathbf{r}'}$. Using Eq.(3) and κ from Eq.(12), we find a non-monotonic T dependence

$$\rho_{21}^{(\mathrm{e})} \propto \frac{T^4}{\left(\Delta_0^2 + \eta(k_B T)^2\right)^3} \langle \delta\mu_1(\mathbf{r}) \delta\mu_2(\mathbf{r}') \rangle_{\mathbf{r}=\mathbf{r}'}, \qquad (13)$$

This dependence is reminiscent of that reported in Ref.[10] for drag resistance at CN. A similar non-monotonic T dependence arises for in-plane resistivity $\Delta\rho_{\alpha\beta}$. At very low T such that $\ell, \tilde{\ell} \gtrsim \xi_{\mathrm{dis}}$, the sum in Eq.(5) is cut at $1/\ell$, giving $\rho_{21} \propto T^8$.

The above analysis can be easily extended to describe the diffusive limit where the elastic mean free path is shorter than the inelastic mean free path, $\ell' < \ell$. Our hydrodynamic approach remains valid in this regime, with the quantity $Q = sT$ where s is the Seebeck coefficient. E-mechanismis still given by Eq.(5), with s and κ described by the Mott and Wiedemann-Franz relations:

$$s = \frac{\pi^2}{3e} k_B^2 T \frac{\partial \ln\sigma}{\partial\mu}, \quad e^2\kappa = \frac{\pi^2}{3} k_B^2 T\sigma, \qquad (14)$$

where σ is the electrical conductivity. Taking σ to vary linearly with carrier density, we find Q that takes on the same qualitative form as Eq.(3) in the clean limit. As a result, the qualitative features of $\rho_{21}^{(\mathrm{e})}$ are similar to those found in the clean limit: namely, the avoided crossing of nodal lines, a peak at zero doping, double sign reversal along the diagonal $n_1 = n_2$ and a three-peak structure along the diagonal $n_1 = -n_2$ (Fig.3(a,b,c)). The T dependence of $\rho_{21}^{(\mathrm{e})}$ (plotted in Fig. 3(d)) is qualitatively similar to the non-monotonic dependence found in the ballistic regime, Eq.(13). However, since the Wiedemann-Franz relation gives $\kappa \propto T$ (in contrast to $\kappa \propto 1/T$ in the ballistic regime), at neutrality we find $\rho_{21}^{(\mathrm{e})} \propto T^2$ at lowest T and $\rho_{21}^{(\mathrm{e})} \propto T^{-4}$ at higher $T \gg \Delta$, as shown in Fig.3(d). Here, we accounted for Dirac point smearing in the same way as in Eqs.(3),(12),(13).

We note that the effects of energy transport, while being completely generic, are particularly strong in graphene. Since P-mechanism vanishes at CN, whereas E-mechanism produces a sharp peak in this region, the latter can be easily discerned even at weak inhomogeneity. The peak structure, the sign and the predicted temperature dependence strikingly resemble experiment[10].

In summary, vertical energy transfer in graphene heterostructures has strong impact on lateral charge transport in the Coulomb drag regime, dominating the drag response at CN. Drag measurements thus afford a unique probe of energy transfer at the nanoscale, a fundamental process which is not easily amenable to more conventional techniques such as calorimetry, and is key for the physics of strong interactions that occur near neutrality.

We acknowledge useful discussions with A. K. Geim, B. Z. Spivak, M. Serbyn and financial support from the NSS program, Singapore (JS), the National Science Foundation Grant No. NSF PHY05-51164 and the Office of Naval Research Grant No. N00014-09-1-0724 (LL).

[1] L. Britnell, R. V. Gorbachev, R. Jalil, B. D. Belle, F. Schedin, A. Mishchenko, T. Georgiou, M. I. Katsnelson, L. Eaves, S. V. Morozov, N. M. R. Peres, J. Leist, A. K. Geim, K. S. Novoselov, and L. A. Ponomarenko, Science **335**, 947 (2012).

[2] W.-K. Tse and S. Das Sarma, Phys. Rev. B **75**, 045333 (2007).

[3] B. N. Narozhny, Phys. Rev. B **76**, 153409 (2007).

[4] R. Sensarma, E. H. Hwang, and S. Das Sarma, Phys. Rev. B **82**, 195428 (2010).

[5] N. M. R. Peres, J. M. B. Lopes dos Santos, and A. H. Castro Neto, Europhys. Lett. **95**, 18001 (2011).

[6] M. I. Katsnelson, Phys. Rev. B **84**, 041407 (2011).

[7] B. N. Narozhny, M. Titov, I. V. Gornyi, and P. M. Ostrovsky, arXiv: 1110.6359 (2012)

[8] T. J. Gramila, J. P. Eisenstein, A. H. MacDonald, L. N. Pfeiffer, and K. W. West Phys. Rev. Lett. **66**, 1216 (1991)

[9] S. Kim, I. Jo, J. Nah, Z. Yao, S. K. Banerjee, and E. Tutuc, Phys. Rev. B **83**, 161401(R) (2011).

[10] R. V. Gorbachev, A. K. Geim, M. I. Katsnelson, K. S. Novoselov, T. Tudoroskiy, I. V. Grigorieva, A. H. MacDonlad, K. Wantanabe, T. Taniguchi, L. A. Ponomarenko, arXiv: 1206.6626 (2012).

[11] U. Sivan, P. M. Solomon, and H. Shtrikman Phys. Rev. Lett. **68**, 1196 (1992)

[12] R. Bistritzer, A. H. MacDonald, Phys. Rev. Lett., **102** 206410 (2009).

[13] W.-K. Tse, S. Das Sarma, Phys. Rev. B, **79**, 235406 (2009).

[14] J. C. W. Song, M. Y. Reizer, and L. S. Levitov, Phys. Rev. Lett., **109** 106602 (2012).

[15] J. Martin, N. Akerman, G. Ulbricht, T. Lohmann, J. H. Smet, K. Von Klitzing, A. Yacoby, Nat. Phys. **4**, 144 (2008).

[16] Y. Zhang, V. W. Brar, C. Girit, A. Zettl, M. F. Crommie, Nat. Physics **6**, 722 (2009).

[17] R. Decker, Y. Wang, V. W. Brar, W. Regan, H. Tsai, Q. Wu, W. Gannett, A. Zettl, and M. F. Crommie, Nano Letters **11**, 4631 (2011)

[18] see Appendix

[19] J.-H. Chen, C. Jang, S. Xiao, M. Ishigami, and M. S. Fuhrer, Nat. Nano. **3**, 206 (2008).

[20] A. V. Andreev, S. A. Kivelson, and B. Spivak Phys. Rev. Lett., **106** 256804 (2011)

[21] K. Nomura, and A. H. MacDonald, Phys. Rev. Lett. **96**, 256602 (2006).

[22] T. Ando, J. Phys. Soc. Jpn. **75**, 074716 (2006).

[23] S. Das Sarma, S. Adam, E. H. Hwang, and E. Rossi, Rev. Mod. Phys. **83**, 407 (2011).

[24] M. Gibertini, A. Tomadin, F. Guinea, M. I. Katsnelson, and M. Polini, Phys. Rev. B **85** 201405 (2012).

[25] S. Das Sarma, E. H. Hwang, and W.-K. Tse, Phys. Rev. B **75**, 121406 (2007).

[26] M. Müller, L. Fritz, and S. Sachdev, Phys. Rev. B. **78**, 115406 (2008)

[27] B. Laikhtman and P. M. Solomon, Phys. Rev. B **41**, 9921 (1990)

[28] See e.g. A. O. Lyakhov, and E. G. Mishchenko, Phys. Rev. B **67** 041304 (2003).